# RSC Advances

ROYAL SOCIETY
OF CHEMISTRY

www.rsc.org/advances

# Facile synthesis of nanostructured LiMnPO₄ as high-performance cathode material with long cycle life and superior rate capability

Longhuan Liao,[a] Jian Xie,[*ab] Shichao Zhang,[c] Gaoshao Cao[b] and Xinbing Zhao[ab]

[a]*State Key Laboratory of Silicon Materials, School of Materials Science and Engineering, Zhejiang University, Hangzhou 310027, P. R. China. E-mail: xiejian1977@zju.edu.cn; Fax: +86-571-87951451; Tel: +86-571-87951451*
[b]*Key Laboratory of Advanced Materials and Applications for Batteries of Zhejiang Province, Hangzhou 310027, P. R. China*
[c]*School of Materials Science and Engineering, Beijing University of Aeronautics and Astronautics, Beijing 100191, P. R. China*

## ABSTRACT

Lithium manganese phosphate (LiMnPO$_4$) has been considered as an alternative to lithium iron phosphate (LiFePO$_4$) for next-generation Li-ion battery cathode because of its higher working voltage. However, facile preparation methods for high-performance LiMnPO$_4$ are still lacking. In this work, we propose a facile route to prepare nano-LiMnPO$_4$ (30–50 nm) by using citric acid (CA) as the surfactant. The addition of a small amount of CA in precursor leads to obvious size reduction of LiMnPO$_4$. After carbon-coated nano-LiMnPO$_4$ exhibits excellent rate capability and long cycle life at high rate because of the small size and uniform/thin carbon coating. At a high rate up to 20 C (3.4 A g$^{-1}$), LiMnPO$_4$/C can still deliver a high discharge capacity of 96.6 mAh g$^{-1}$. LiMnPO$_4$/C also exhibits long cycle life with ~70% capacity retained after 500 cycles at 10 C. The excellent electrochemical performance of LiMnPO$_4$/C makes it attractive cathode in high-power and high-energy Li-ion batteries.

2

## 1. Introduction

$LiMPO_4$ (M = Fe, Mn, Co) with an olivine-type structure has gained a wide interest as new cathode materials for Li-ion batteries since the first report on $LiFePO_4$ by Goodenough and co-workers in 1997.[1] In these olivine-type materials, $LiFePO_4$ has now realized practical applications in electric vehicles (EVs) because of its environmental friendliness, low cost and structural stability.[2,3] Compared with $LiFePO_4$, $LiMnPO_4$ (LMP) could provide a larger energy density with its higher redox potential of $Mn^{2+}/Mn^{3+}$ (4.1 V *vs.* $Li/Li^+$) than $Fe^{2+}/Fe^{3+}$ (3.45 V *vs.* $Li/Li^+$).[4–6] However, $LiMnPO_4$ exhibits a rather lower electrochemical activity than $LiFePO_4$ due to its intrinsically lower electronic and ionic conductivity,[7,8] structural instability of $MnPO_4$ phase,[9,10] and larger volume change between $LiMnPO_4$ and $MnPO_4$.[11] In addition, The $Mn^{3+}$ in the charge state undergoes Jahn-Teller distortion.[12,13] In recent years, great effort has been made to improve the electrochemical activity of $LiMnPO_4$ through cation substitution, size decrease, optimized carbon coating, etc.[14] Cation substitution has found to be an effective measure to activate $LiMnPO_4$ and stabilize the delithiated phase.[15] However, the substitution should be controlled at a low level to maintain the high energy density of $LiMnPO_4$.[16–24]

Size decrease is another useful method to enhance the electrochemical activity of $LiMnPO_4$. Oh et al. synthesized $LiMnPO_4$ using a spray-pyrolysis/ball-milling route.[25] The $LiMnPO_4$ of 10–50 nm could deliver high capacities of 158 mAh $g^{-1}$ at 0.05 C and 126 mAh $g^{-1}$ at 1 C after coating of uniform carbon layer. Recent work has shown that nano-engineering could remarkably improve the electrochemical performance of $LiMnPO_4$.[18,26–42] Since Yang et al. first reported the direct synthesis of $LiFePO_4$ by hydrothermal method,[43] hydrothermal/solvothermal route has been widely used to prepare $LiMPO_4$ (M = Fe, Mn) with nanostructure.[44] The size and morphology of $LiMnPO_4$ could be easily regulated by controlling the synthetic conditions (temperature, time, reactant concentration/ratio, etc) and using different solvents or surfactants.[26–29,35–39] The work by Qin et al. indicated that the morphology of $LiMnPO_4$ can be controlled by simply adjusting the pH value.[27] The obtained $LiMnPO_4$ nanoplates could yield high capacities of 149 mAh $g^{-1}$ at 0.1 C and 90 mAh

g$^{-1}$ at 1 C after graphene coating. Hong et al. synthesized LiMnPO$_4$ nanorods by setting the volume ratio of ethylene glycol (EG) and water at 11:1.[37] The carbon-coated LiMnPO$_4$ could deliver a high capacity of 110 mAh g$^{-1}$ at 10 C and a capacity retention of ~94.5% after 100 cycles at 0.5 C.

It is generally accepted that, nano-engineering is a practical strategy to realize the high performance of LiMnPO$_4$ materials. Nevertheless, a challenge still remains to find a facile preparation method for nanosized LiMnPO$_4$. For the solvothermal synthesis of LiMnPO$_4$, the reaction of H$_3$PO$_4$ + 3LiOH + MnSO$_4$ = LiMnPO$_4$ + Li$_2$SO$_4$ + 3H$_2$O is usually adopted. The morphology of LiMnPO$_4$ was found to depend greatly on molar ratios of H$_3$PO$_4$/LiOH/MnSO$_4$.[27,39] Actually, acidity plays a critical role in determining the morphology of LiMnPO$_4$ in the reactions. In this work, nanostructured LiMnPO$_4$ was prepared by a facile solvothermal route in an EG/H$_2$O mixed solvent with citric acid (CA) as a surfactant. The results showed that the addition of a small amount of CA leads to an obvious size decrease and considerable performance improvement of LiMnPO$_4$. The LiMnPO$_4$/C granules of 30–50 nm could deliver high capacities of 147.9, 113.0 and 96.6 mAh g$^{-1}$ at 1 C, 10 C and 20 C, respectively. The capacities can be retained at 89.1 and 80.5 mAh g$^{-1}$ after 500 cycles at 1 C and 10 C, respectively. The intrinsic mechanism for performance enhancement was also investigated by cyclic voltammetry (CV) and electrochemical impedance spectroscopy (EIS). This work provides a facile method to realize a high performance of the LiMnPO$_4$ materials.

## 2. Experimental Section

### 2.1 Preparation of LiMnPO$_4$ and LiMnPO$_4$/C

LiMnPO$_4$ was prepared by a facile solvothermal route via reaction H$_3$PO$_4$ + 3LiOH + MnSO$_4$ = LiMnPO$_4$ + Li$_2$SO$_4$ + 3H$_2$O in an EG/water mixed solvent.[39] The molar ratio of H$_3$PO$_4$, LiOH and MnSO$_4$ in the precursor is 1:3:1. During the preparation of the MnSO$_4$ solution in EG/water, a desired amount of CA (1–7 mmol) was added. The reaction products are named LMP-$x$, where $x$ represents the amount of CA used (in the unit of mmol). For example, when 1.0 mmol of CA was used, the product is named LMP-1.0. The carbon coating procedure was conduced according to the

previous work.[39] For simplicity, $LiMnPO_4/C$ uses the same name as the corresponding $LiMnPO_4$ sample.

## 2.2 Materials characterization

X-ray diffraction (XRD) patterns were collected on a Rigaku D/Max-2550pc powder diffractometer (Cu $K_{\alpha}$, $\lambda$ = 0.1541 nm) to analyze the crystalline structure of $LiMnPO_4$. The morphology and microstructure of $LiMnPO_4$ and $LiMnPO_4/C$ were checked by scanning electron microscope (SEM) on an S-4800 microscope and transmission electron microscopy (TEM) on a JEM 2100F microscope. Carbon content in $LiMnPO_4/C$ samples was obtained using a Flash EA 1112 tester. In the equipment, the solid carbon can be combusted into gaseous $CO_2$ in a rapid and dynamic mode. The carbon content can be determined by analyzing the amount of $CO_2$ with chromatography. The Brunauer-Emmett-Teller (BET) specific surface area of $LiMnPO_4$ was calculated based on the $N_2$ absorption/desorption isotherms using a Quantachrome Autosorb-1 analyser.

## 2.4 Electrochemical measurements

The electrochemical performance of $LiMnPO_4/C$ was measured using CR2025-type coin cells on a Neware battery cycler (Shenzhen, China). The electrode was made by homogeneously mixing $LiMnPO_4/C$, acetylene black and polyvinylidene fluoride in a mass ratio of 7:2:1. The active material ($LiMnPO_4/C$) loading was around 2 mg. The cells assembly was conducted in a glove box filled with pure Ar. For the cells, metallic Li foils were used as the counter electrodes, 1 M $LiPF_6$ in ethylene carbonate (EC)/dimethyl carbonate (DMC) (1:1 by volume) was used as the electrolyte, and Celgard 2300 microporous membranes were used as the separators. The cells were tested with a constant-current–constant-voltage (CC–CV) protocol. The cells were first galvanostatically charged to 4.5 V at different current rates, then held at 4.5 V for 1 h, and galvanostatically discharged to 2.0 V. The charge and discharge processes use the same current rate. The current density was calculated based on the total mass of $LiMnPO_4$ and carbon for the $LiMnPO_4/C$ composites. The specific capacity of $LiMnPO_4/C$ is normalized by the mass of $LiMnPO_4$ and 1 C is defined as 170 mA $g^{-1}$. CV tests were conducted at 2.0−4.5 V (*vs.* Li/Li$^+$) with a scan rate of 0.1 mV $s^{-1}$ on a VersaSTAT3

electrochemistry workstation (Princeton Applied Research). EIS tests were carried out on the VersaSTAT3 workstation using an ac voltage of 10 mV amplitude in a frequency range of 10 mHz – 100 kHz. The EIS measurements were performed in the lithiated state of $LiMnPO_4$ after the rest of the cells for several hours. The electrochemical tests were performed at room temperature.

## 3. Results and discussion

Fig. 1 gives XRD patterns of the solvothermal products with different amounts of CA in the precursors. The phase purity of the $LiMnPO_4$ samples was confirmed by comparing with the standard diffraction peaks of $LiMnPO_4$ (Space group *pnmb*, JCPDS Card no. 33−0804). Note that the relative intensity of the diffraction peaks changes with increasing the CA amount, suggesting the changes of morphology and size of $LiMnPO_4$. The sharp peaks suggest a high crystallinity of $LiMnPO_4$ samples even they were prepared at low temperature.
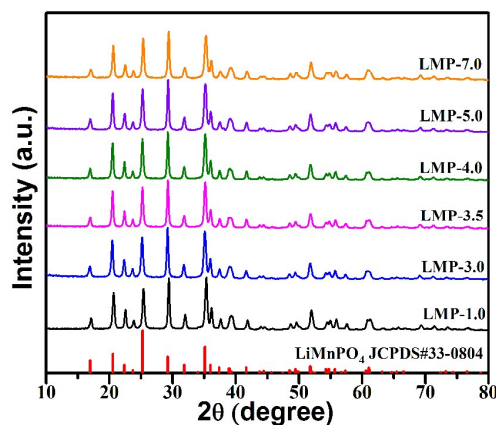


**Fig. 1** XRD patterns of $LiMnPO_4$ prepared with different CA amounts in the precursors.

The morphology of the solvothermal products was characterized by SEM. The $LiMnPO_4$ exhibits a spindle-like shape when it was prepared with a CA-free precursor (Fig. S1). The size of the spindle-like $LiMnPO_4$ is around 200 nm and the BET specific surface area is 32.2 $m^2g^{-1}$. As seen in Fig. 2a, the shape and size of $LiMnPO_4$ show a remarkable change when a small amount of CA (CA/$MnSO_4$ molar ratio is 1/10) was added in the precursor. The obtained $LiMnPO_4$ demonstrates a plate-like shape with a size below 100 nm. The size of $LiMnPO_4$ can be further

reduced to 30–50 nm by increasing the CA amount (CA/MnSO$_4$ molar ratio is 3/10). The LiMnPO$_4$ exhibits an irregular granule shape with BET surface area increased to 53.8 m$^2$g$^{-1}$ (Fig. 2b). The size of LiMnPO$_4$ shows a trend to increase when the amount of CA was further increased (Fig. 2c−f). At a CA/MnSO$_4$ molar ratio of 7/10, the LiMnPO$_4$ crystallizes into plate-like shape again and the surface area decreases to 45.7 m$^2$g$^{-1}$ (Fig. 2f). Even so, the plate-like LiMnPO$_4$ still has a smaller size than the spindle-like one, suggesting that CA does plays a critical role in reducing the size of LiMnPO$_4$. The size decrease, in turn, will enhance the electrochemical performance of LiMnPO$_4$, which will be discussed later.
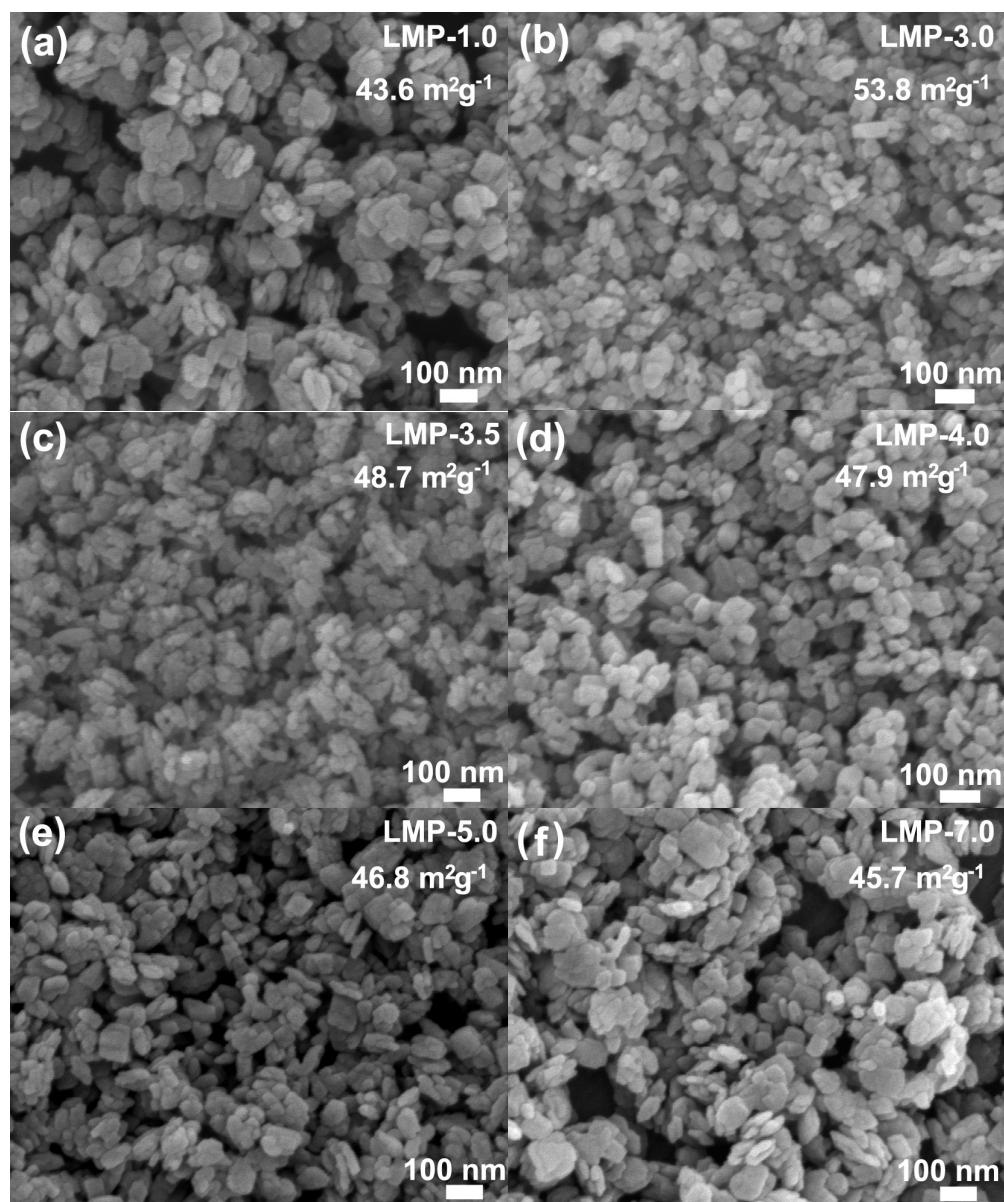
**Fig. 2** SEM images of LiMnPO$_4$ prepared with different CA/MnSO$_4$ molar ratios in the precursors:

(a) 1/10, (b) 3/10, (c) 7/20, (d) 2/5, (e) 1/2 and (f) 7/10.

Fig. 3 presents TEM images of the pristine LMP-3.0 and carbon-coated LMP-3.0. As seen in Fig. 3,b, the pristine LMP-3.0 exhibits an irregular shape with a size of 30–50 nm, agreeing with the SEM observation. The morphology of the sample was retained after carbon coating as shown in Fig. 3c. High-resolution TEM (HRTEM) image in Fig. 3d indicates that the LiMnPO$_4$ is well crystallized. The lattice spacings of 0.21 and 0.36 nm related to the (112) and (111) planes of LiMnPO$_4$. The surface of LiMnPO$_4$ is uniformly coated by a layer of carbon with a thickness ~1 nm. As a result, size decrease of LiMnPO$_4$ has realized through a facile solvothermal route using CA as the surfactant. The mechanism is schematically illustrated in Fig. 4. The adsorption of CA on the surface of LiMnPO$_4$ inhibits its continuous growth during the solvothermal reaction. The LiMnPO$_4$ grows into irregular shape due possibly to the different adsorption ability of CA on the different crystalline planes of LiMnPO$_4$. However, excess CA will greatly change the acidity of the solution, leading to the formation of plate-like LiMnPO$_4$, similar to the case in H$_3$PO$_4$ where excess H$_3$PO$_4$ also results in the crystal growth of LiMnPO$_4$.[39]
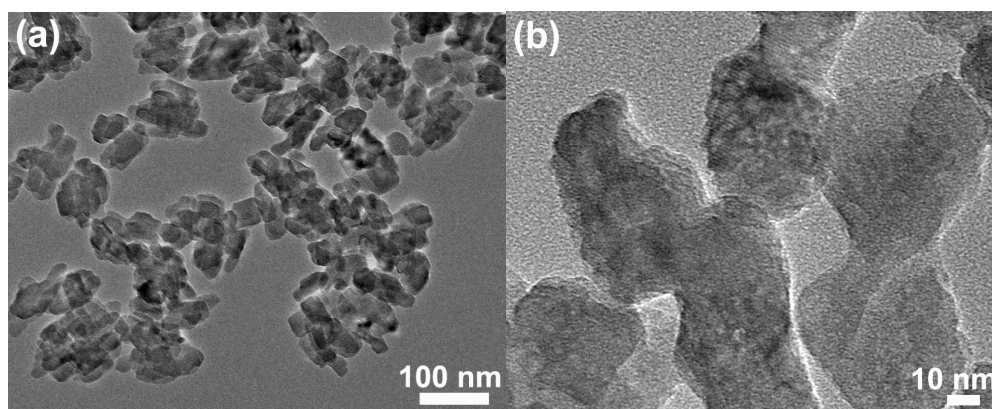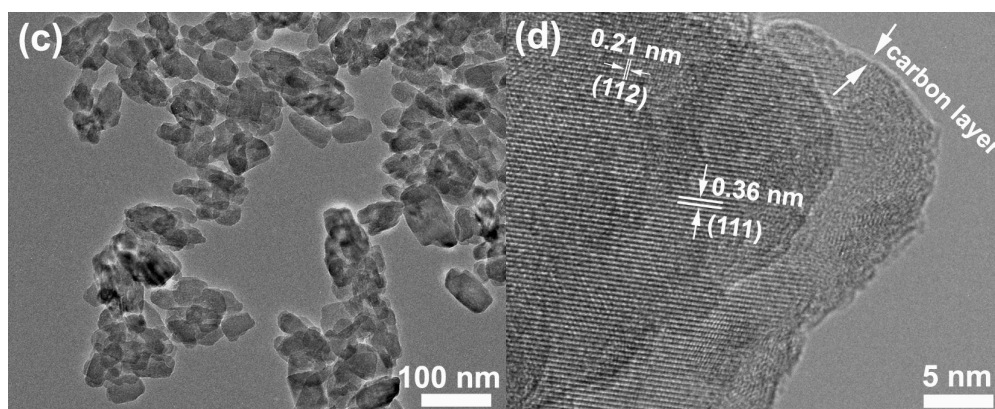
**Fig. 3** TEM images of (a, b) pristine and (c, d) carbon-coated LMP-3.0.
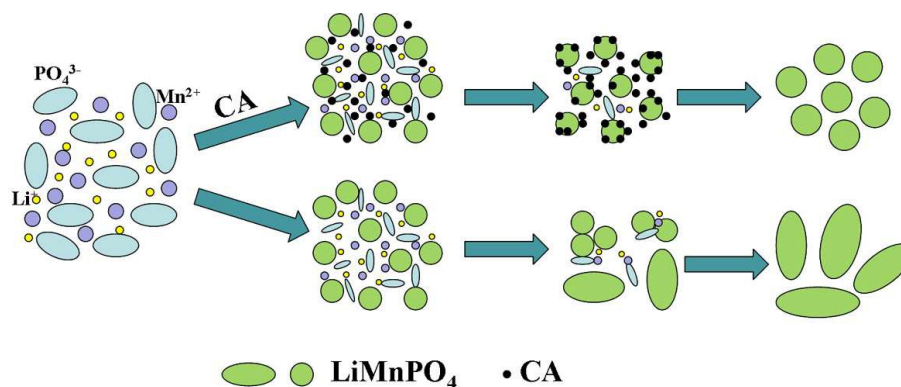


**Fig. 4** Schematic illustration of the CA-induced refrained growth of LiMnPO₄ crystals.

Electrochemical tests were performed on three LiMnPO₄/C samples with different sizes to reveal the size dependence of the electrochemical performance. Fig. 5a gives the first charge-discharge curves of the LiMnPO₄/C samples at 0.05 C. The capacities of LiMnPO₄/C were calculated normalized to the mass of LiMnPO₄. As seen in the figure, these samples exhibit high electrochemical activity at a low current rate, delivering high discharge capacities (164.5 mAh g$^{-1}$ for LMP-3.0, 163 mAh g$^{-1}$ for LMP-3.5, 161 mAh g$^{-1}$ for LMP-4.0). Specially, LMP-3.0 yields the highest discharge capacity of 164.5 mAh g$^{-1}$, which is close to the theoretical capacity of LiMnPO₄ (170 mAh g$^{-1}$). The highest capacity of LMP-3.0 is closely correlated with its smallest crystal size which maximizes the utilization of active material. For LiMnPO₄ material, irreversible capacities in the first cycle are usually observed, which is attributed to the passivation of the electrolyte and electrode at high potentials.[37,45] The irreversible capacities of LMP-3.0, LMP-3.5 and LMP-4.0 are 17.5, 19 and 24 mAh g$^{-1}$, respectively. Fig. 5b shows the CV scans of the samples at 0.1 mV s$^{-1}$.

LMP-3.0 displays obviously stronger and sharper current peaks than LMP-3.5 and LMP-4.0, indicating its fastest electrochemical reaction kinetics due to the smallest crystal size.
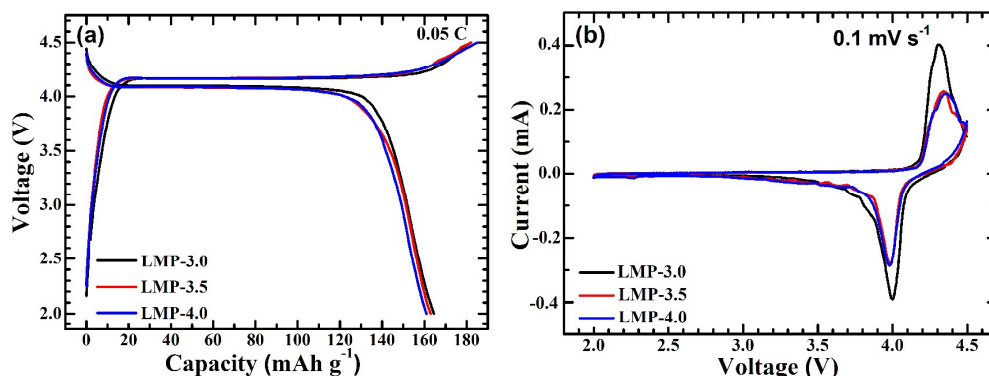


**Fig. 5** (a) Voltage profiles and (b) CV plots of the carbon-coated LiMnPO$_4$.

Fig. 6 compares the rate capability of the LiMnPO$_4$/C samples at current rates of 0.1 C−20 C. The charge and discharge processes of the cells were performed at the same current rates in the rate capability tests. Note that the plateau length is on the decrease with the increase in current rate. The polarization also increases with increasing the current density. LMP-3.0 shows the best rate capability among the three samples. The discharge capacities of LMP-3.0 are 158.6, 152.3, 147.9, 140.0 and 126.1 mAh g$^{-1}$ at 0.1 C, 0.5 C, 1 C, 2 C and 5 C, respectively. At 10 C and 20 C, this sample can still deliver high capacities of 113.0 and 96.6 mAh g$^{-1}$, respectively. The superior rate capability of LMP-3.0 can be ascribed to its small crystal size and uniform/thin conductive carbon layer, making it possible for rapid electron and Li-ion transport. The LMP-3.0 sample shows a slower capacity decrease with current density than LMP-3.5 and LMP-4.0 especially at high current densities, implying that the crystal size does exert an obvious effect on the Li-ion transport on the electrode/electrolyte interface and in bulk crystals.
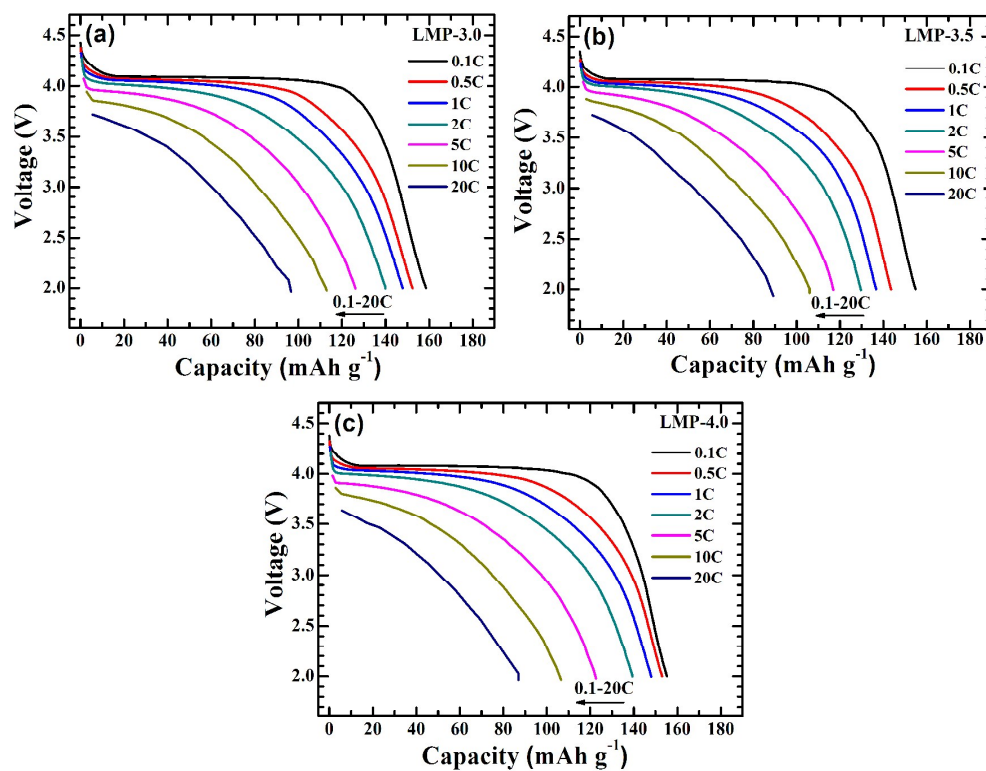
**Fig. 6** Rate capability of LiMnPO$_4$/C: (a) LMP-3.0, (b) LMP-3.5 and (c) MP-4.0.

Fig. 7 demonstrates the cycling stability of the LiMnPO$_4$/C samples. As seen in Fig. 7a, LMP-3.0, LMP-3.5 and LMP-4.0 can deliver high initial discharge capacities of 147.2, 142.8 and 142.6 mAh g$^{-1}$ at 1 C, which can be maintained at 89.1, 84.3 and 75.1 mAh g$^{-1}$ after 500 cycles. LMP-3.0 exhibits the best cycling stability with a capacity retention over 60% after 500 cycles at 1 C. Even after 500 cycles at 10 C, this sample can still keep a discharge capacity of 80.5 mAh g$^{-1}$, with a retention around 70%. Although the cycling stability of LiMnPO$_4$/C has been enhanced by various strategies in recent work,[25–30,32, 33,35–37,41, 42] there are few reports on LiMnPO$_4$/C that can sustain 500 cycles at such a high current density (10 C). It should be stressed that the charge and discharge in this work were performed at the same current rate. The outstanding cycling stability of LMP-3.0 can be due to the uniform carbon coating which refrains Mn dissolution,[25,34,42,45] and small crystal size which alleviates volume strain between LiMnPO$_4$ and MnPO$_4$.[11,42,46,47] In contrast, the large-sized spindle-like LiMnPO$_4$ exhibits low capacity and poor cycling stability (Fig. S2). The low capacity and poor cycling stability of spindle-like LiMnPO$_4$ can be attributed to the low Li-ion

diffusion rate with insufficient utilization of active material and poor carbon coating for large-sized $LiMnPO_4$ particles. Table 1 compares the rate capability and cycle life of some $LiMnPO_4/C$ composites in this work and others. The data summarized in Table 1 represent the best ones on $LiMnPO_4/C$ materials reported to date. Of note is that both rate capability and cycle life of our LMP-3.0 sample are among the best ones when we compare charge/discharge mode, applied current rate and cycle number comprehensively. We propose that the outstanding electrochemical properties of our $LiMnPO_4/C$ can be attributed to the small size and uniform carbon coating, which renders rapid electron and Li-ion transport and easy release of the lattice strain upon repeated cycling. The carbon coating also led to remarkably improved electrochemical performance of other cathode materials such as $LiNi_{0.8}Co_{0.1}Mn_{0.1}O_2$ and $LiNi_{0.5}Mn_{1.5}O_4$ by stabilizing the structure and supplying the conducting channels.[48,49] In addition, the ultrathin carbon layer facilitates Li-ion diffusion across electrode/electrolyte interface with enhanced electrode kinetics. It should be noted that the $LiMnPO_4/C$ in our work was prepared by a facile solvothermal route using small amounts of inexpensive and nontoxic citric acid.
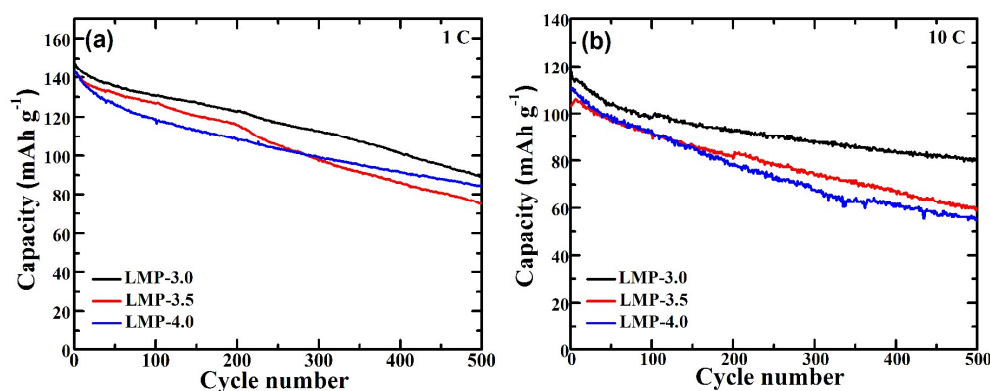


**Fig. 7** Cycling stability of $LiMnPO_4/C$ at (a) 1 C and (b) 10 C.

**Table 1** Comparison of electrochemical performance of LiMnPO$_4$/C in this work with others.

| Sample and preparation method | Cycling stability | | | | Rate capability | | | | Reference |
|---|---|---|---|---|---|---|---|---|---|
| | Current density | Initial capacity (mAh g$^{-1}$) | Cycle number | Capacity retention | Current density / Capacity (mAh g$^{-1}$) | | | | |
| **LMP-3.0, SR with CA** | **10C-ch, 10C-dis** | **117.6** | **100/500** | **83%/68%** | **1C-ch, 1C-dis** **147.9** | **5C-ch, 5C-dis** **126.1** | **10C-ch, 10C-dis** **113.0** | **20C-ch, 20C-dis** **96.6** | **This work** |
| LMP, spray pyrolysis and BM | 0.05C-ch, 0.5C-dis | ~140 | 50 | 94.2% | 0.05C-ch, 1C-dis 126 | 0.05C-ch, 2C-dis 107 | 0.05C-ch, 10C-dis ~60 | | [25] |
| LMP plates, SR with SDBS | 0.05C-ch, 0.05C-dis | 147 | 50 | 93% | 0.1C-ch, 1C-dis ~110 | 0.1C-ch, 2C-dis ~95 | 0.1C-ch, 5C-dis ~70 | | [26] |
| LMP/G, SR+ spray drying | 1C-ch-dis, 2C-ch-dis, 5C-ch-dis | ~90 | 60 | 75% | 1C-ch, 1C-dis 90 | 2C-ch, 2C-dis ~75 | 5C-ch, 5C-dis 64 | | [27] |
| LMP grains, SR with CTAB | 0.05C-ch, 0.05C-dis | 153 | 110 | 95.4% | 0.05C-ch, 1C-dis 128 | 0.05C-ch, 5C-dis 111 | 0.05C-ch, 10C-dis 92 | | [28] |
| LMP, precipitation+BM | 0.05C-ch, 0.2C-dis | ~135 | 45 | 90.5% | 0.05C-ch, 1C-dis 120 | 0.05C-ch, 5C-dis 90 | 0.05C-ch, 10C-dis 61 | | [30] |
| porous LMP, PMMA template | | – | | | 0.1C-ch, 1C-dis 154 | 0.1C-ch, 6C-dis 129 | 0.1C-ch, 10C-dis 110 | | [31] |
| LMP sheets, SR with HT, HP and PVP | 0.2C-ch, 0.2C-dis | 157 | 50 | 93.6% | 5C-ch, 5C-dis 119 | 10C-ch, 10C-dis 93 | 20C-ch, 20C-dis 63 | | [32] |
| LMP granules, SSR with OA | 0.1C-ch-dis, 0.2C-ch/ 0.5C-dis | 122 | 50+50 | 97.5% +96.4% | 0.05C-ch, 5C-dis 95.7 | 0.05C-ch, 10C-dis 87.1 | 0.05C-ch, 20C-dis 60.1 | | [33] |
| LMP plates, SR with CTAB | 0.2C-ch, 1C-dis | 130.3 | 500 | 92.7% | 1C-dis 127.6 | 5C-dis 93.8 | 10C-dis 69.2 | | [35] |
| LMP, SR | 0.5C-ch, 0.5C-dis | 138 | 100 | 91.5% | 1C-ch, 1C-dis ~135 | 5C-ch, 5C-dis 118 | 10C-ch, 10C-dis 106 | | [36] |
| LMP rods, SR | 0.5C-ch, 0.5C-dis | 144.5 | 100 | 94.5% | 1C-ch, 1C-dis 137 | 5C-ch, 5C-dis ~125 | 10C-ch, 10C-dis 110 | | [37] |
| LMP flakes, SR+sintering | 0.5C-ch, 0.5C-dis | ~135 | 200 | >95% | 1C-ch, 1C-dis 130 | 5C-ch, 5C-dis 110 | 10C-ch, 10C-dis 92 | | [40] |
| LMP, BM+SSR | 1C-ch, 1C-dis | 128 | 200 | 94% | 0.1C-ch, 1C-dis >120 | 0.1C-ch, 2C-dis ~105 | 0.1C-ch, 5C-dis ~60 | | [42] |

Note: SR=solvothermal reaction, SSR=solid state reaction, BM=ball milling, HT=high temperature, HP=high pressure, ch=charge, dis=discharge, LMP=LiMnPO$_4$, SDBS=sodium dodecyl benzene sulfonate, G=grapheme, CTAB=hexadecyltrimethyl ammonium bromide, PMMA=polymethyl methacrylate, PVP=polyvinylpyrrolidone, OA=oleic acid

EIS tests were used to reveal the different electrode kinetics among the three samples. As seen in Fig. 8a, the Nyquist plots of the LiMnPO$_4$/C samples are constructed by a high-frequency semicircle and a low-frequency slopping line. The plots were fitted by the equivalent circuit (see inset in Fig. 8a). In the circuit, $R_e$ denotes the electrolyte and ohm resistance, $R_i$ and $Q_1$ are related to contact resistance of active material with the current collector and the related capacitance, respectively, $R_{ct}$ and $Q_2$ represent charge transfer resistance and double-layer capacitance, respectively, and $Z_w$ is the Warburg impedance related to Li-ion bulk diffusion.[50–52] As shown in the Table 2, LMP-3.0 exhibits much lower $R_{ct}$ value compared with LMP-3.5 and LMP 4.0 although they have similar $R_i$ values. The low $R_{ct}$ value means rapid electrochemical reaction kinetics on the electrode/electrolyte interface, which is closely related to the uniform/thin conductive carbon layer and large specific surface area of LMP-3.0.

Li-ion chemical diffusion coefficients $D_{Li}$ were also measured using EIS to further understand the different electrochemical behaviors between these LiMnPO$_4$/C samples. To calculate the $D_{Li}$ values using the EIS technique, the Warburg factor $\sigma$ in the Warburg region should first be determined. Fig. 8b shows the Nyquist plot of LMP-3.0 with marked frequency $f$ and the Warburg region with a slope of ~45$^o$. The inset in Fig. 8b correlates $Z'$ (or $–Z'$) with $\omega^{-1/2}$ ($\omega = 2\pi f$) where $\sigma$ can be obtained by linearly fitting the $Z'$ (or $–Z'$) $vs.$ $\omega^{-1/2}$ plots. Thus, $D_{Li}$ (cm$^2$ s$^{-1}$) values can be calculated using the following equation: [33,53,54]

$$D_{Li} = R^2T^2/(2A^2n^4F^4C^2\sigma^2) \tag{1}$$

where $R$ is the gas constant, $T$ is the absolute temperature (K), $A$ is the surface area of the electrode (cm$^2$), $n$ is number of transferred electrons per LiMnPO$_4$ molecule upon complete delithiation, $F$ is the Faraday constant, $C$ is the Li-ion concentration in LiMnPO$_4$ (0.022 mol cm$^{-3}$), and $\sigma$ is the Warburg factor ($\Omega$ Hz$^{1/2}$). The $D_{Li}$ values of the three samples are listed in Table 2. We can see that LMP-3.0 has a higher $D_{Li}$ value than the other samples, implying the rapidest Li-ion bulk diffusion. This can explain its better rate capability and enhanced high-rate cycling stability. The EIS results are consistent with the different electrochemical behaviors of the three samples.
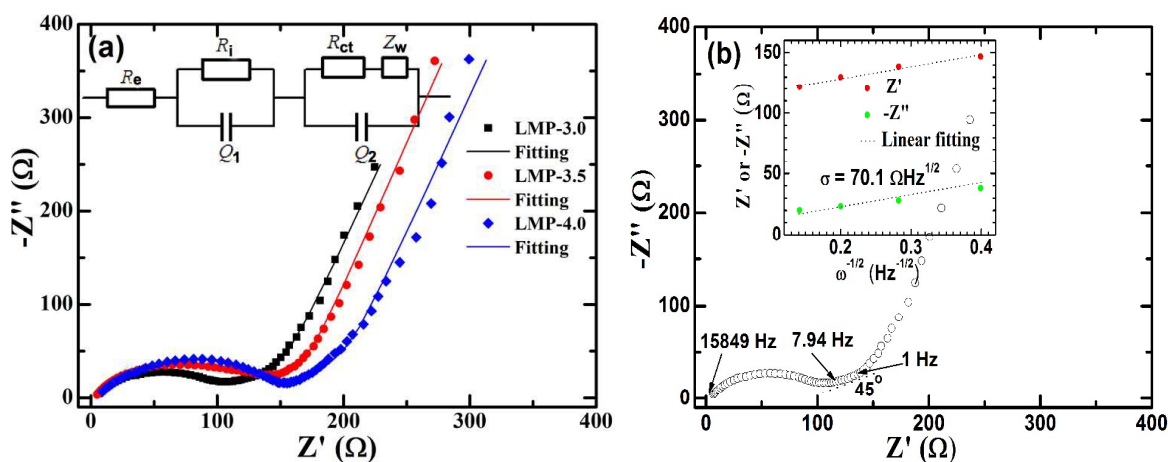
**Fig. 8** (a) Nyquist plots and equivalent circuit of LiMnPO$_4$/C and (b) $Z'$ (or $-Z''$) $vs.$ $\omega^{-1/2}$ plots and the linear fitting of carbon-coated LMP-3.0 in the Warburg region.

**Table 2** Fitting results of the Nyquist plots using the equivalent circuit and the $D_{Li}$ values.

| Sample | $R_e$ (Ω) | $R_i$ (Ω) | $Q_1$ | | $R_{ct}$ (Ω) | $Q_2$ | | $D_{Li}$ (cm$^2$ s$^{-1}$) |
|--------|-----------|-----------|-------|-------|--------------|-------|-------|----------------------------|
| | | | $Y$ | $n$ | | $Y$ | $n$ | |
| LMP-3.0 | 3.2 | 88.5 | $9.3\times10^{-5}$ | 0.58 | 25.4 | $1.6\times10^{-5}$ | 0.77 | $5.0\times10^{-15}$ |
| LMP-3.5 | 2.2 | 84.8 | $6.5\times10^{-4}$ | 0.54 | 93.4 | $2.2\times10^{-5}$ | 0.68 | $1.6\times10^{-15}$ |
| LMP-4.0 | 2.7 | 84.7 | $5.9\times10^{-4}$ | 0.58 | 117.3 | $2.1\times10^{-5}$ | 0.67 | $2.9\times10^{-15}$ |

## 4. Conclusions

In summary, we proposed a facile solvothermal route to synthesize LiMnPO$_4$ nanocrystals by using CA as the surfactant. The morphology and size of LiMnPO$_4$ change greatly by adding a small amount of CA, which realizes the conversion of spindle-like LiMnPO$_4$ of 200 nm into granule-like one of 30–50 nm. The LiMnPO$_4$ granules display superior rate capability and cycling stability at high rates after the coating of a uniform/thin carbon layer of ~1 nm thickness. At 20 C, a high discharge capacity of 96.6 mAh g$^{-1}$ can be achieved for LiMnPO$_4$/C. The excellent rate capability is attributed to the small size with easy Li-ion transport on electrode/electrolyte interface and in bulk material, and to the uniform/thin carbon layer with enhanced electron transport. The LiMnPO$_4$/C granules also show outstanding high-rate cycling stability with a discharge capacity of 80.5 mAh g$^{-1}$ maintained after 500 cycles at 10 C. The long cycle life is ascribed to the small size which alleviates the lattice strains and the uniform carbon coating which refrains the Mn dissolution. The superior electrochemical performance of LiMnPO$_4$/C makes it promising applications in EVs.

## Acknowledgements

## Notes and references

1 A. K. Padhi, K. S. Nanjundaswamy and J. B. Goodenough, *J. Electrochem.Soc.*, 1997, **144**, 1188–1194.

2 L. X. Yuan, Z. H. Wang, W. X. Zhang, X. L. Hu, J. T. Chen, Y. H. Huang and J. B. Goodenough, *Energy Environ. Sci.*, 2011, **4**, 269–284.

3 O. K. Park, Y. Cho, S. Lee, H. C. Yoo, H. K. Song and J. Cho, *Energy Environ. Sci.*, 2011, **4**, 1621–1633.

4 C. Delacourt, P. Poizot, M. Morcrette, J. M. Tarascon and C. Masquelier, *Chem. Mater.*, 2004, **16**, 93–99.

5 M. Yonemura, A. Yamada, Y. Takei, N. Sonoyama and R. Kanno, *J. Electrochem. Soc.*, 2004, **151**, A1352–A1356.

6 F. Zhou, M. Cococcioni, K. Kang and G. Ceder, *Electrochem. Commun.*, 2004, **6**, 1144–1148.

7 C. Delacourt, L. Laffont, R. Bouchet, C. Wurm, J. B. Leriche, M. Morcrette, J. M. Tarascon and C. Masqueliera, *J. Electrochem. Soc.*, 2005, **152**, A913–A921.

8 D. Morgan, A. Van der Ven and G. Ceder, *Electrochem. Solid-State Lett.*, 2004, **7**, A30–A32.

9 A. Yamada, M. Yonemura, Y. Takei, N. Sonoyama and R. Kanno, *Electrochem, Solid-State Lett.*, 2005, **8**, A55–A58.

10 D. Choi, J. Xiao, Y. J. Choi, J. S. Hardy, M. Vijayakumar, M. S. Bhuvaneswari, J. Liu, W. Xu, W. Wang, Z. G. Yang, G. L. Graff and J. G. Zhang, *Energy Environ. Sci.*, 2011, **4**, 4560–4566.

11 N. Meethong, H. Y. Shadow Huang, S. A. Speakman, W. Craig Carter and Y. M. Chiang, *Adv.*

*Funct. Mater.*, 2007, **17**, 1115–1123.

12 L. F. J. Piper, N. F. Quackenbush, S. Sallis, D. O. Scanlon, G. W. Watson, K. W. Nam, X. Q. Yang, K. E. Smith, F. Omenya, N. A. Chernova and M. S. Whittingham, *J. Phys. Chem. C*, 2013, **117**, 10383−10396.

13 Y. Mishima, T. Hojo, T. Nishio, H. Sadamura, N. Oyama, C. Moriyoshi and Y. Kuroiwa, *J. Phys. Chem. C*, 2013, **117**, 2608−2615.

14 V. Aravindan, J. Gnanaraj, Y. S. Lee and S. Madhavi, *J. Mater. Chem. A*, 2013, **1**, 3518–3539.

15 G. Y. Chen, J. D. Wilcox and T. J. Richardson, *Electrochem. Solid-State Lett.*, 2008, **11**, A190–A194.

16 P. F. Xiao, B. Ding, M. O. Lai and L. Lu, *J. Electrochem. Soc.*, 2013, **160**, A918–A926.

17 V. Ramar and P. Balaya, *Phys. Chem. Chem. Phys.,* 2013, **15**, 17240–17249.

18 S. Liu, H. S. Fang, E. R. Dai, B. Yang, Y. C. Yao, W. H. Ma and Y. N. Dai, *Electrochim. Acta*, 2014, **116**, 97−102.

19 Q. Lu, G. S. Hutchings, Y. Zhou, H. L. Xin, H. M. Zheng and F. Jiao, *J. Mater. Chem. A*, 2014, **2**, 6368–6373.

20 M. S. Kim, J. P. Jegal, K. C. Roh and K. B. Kim, *J. Mater. Chem. A*, 2014, **2**, 10607–10613.

21 K. Kisu, E. Iwama, W. Onishi, S. Nakashima, W. Naoi and K. Naoi, *J. Mater. Chem. A*, 2014, **2**, 20789–20798.

22 L. J. Hu, B. Qiu, Y. G. Xia, Z. H. Qin, L. F. Qin, X. F. Zhou and Z. P. Liu, *J. Power Sources*, 2014, **248**, 246–252.

23 X. Zhou, Y. F. Deng, L. N. Wan, X. S. Qin and G. H. Chen, *J. Power Sources*, 2014, **265**, 223–230.

24 P. J. Zuo, L. G. Wang, W. Zhang, G. P. Yin, Y. L. Ma, C. Y. Du, X. Q. Cheng and Y. Z. Gao, *Nanoscale*, 2015, **7**, 11509–11514.

25 S. M. Oh, S. W. Oh, C. S. Yoon, B. Scrosati, K. Amine and Y. K. Sun, *Adv. Funct. Mater.*, 2010, **20**, 3260–3265.

**RSC Advances Accepted Manuscript**

26 F. Wang, J. Yang, P. F. Gao, Y. NuLi and J. L. Wang, *J. Power Sources*, 2011, **196**, 10258–10262.

27 Z. H. Qin, X. F. Zhou, Y. G. Xia, C. L. Tang and Z. P. Liu, *J. Mater. Chem.*, 2012, **22**, 21144–21153.

28 H. C. Dinh, S. I. Mho, Y. Kang and I. H. Yeo, *J. Power Sources*, 2013, **244**,189–195.

29 S. L. Yang, R. G. Ma, M. J. Hu, L. J. Xi, Z. G. Lu and C. Y. Chung, *J. Mater. Chem.*, 2012, **22**, 25402–25408.

30 K. Su, F. Liu and J. T. Chen, *J. Power Sources*, 2013, **232**, 234–239.

31 H. Yoo, M. Jo, B. S. Jin, H. S. Kim and J. Cho, *Adv. Energy Mater.*, 2011, **1**, 347–351.

32 X. H. Rui, X. X. Zhao, Z. Y. Lu, H. T. Tan, D. H. Sim, H. H. Hng, R. Yazami, T. M. Lim and Q. Y. Yan, *ACS Nano*, 2013, **7**, 5637–5646.

33 L. F. Zhang, Q. T. Qu, L. Zhang, J. Li and H. H. Zheng, *J. Mater. Chem. A*, 2014, **2**, 711–719.

34 L. G. Wang, P. J. Zuo, G. P. Yin, Y. L. Ma, X. Q. Cheng, C. Y. Du and Y. Z. Gao, *J. Mater. Chem. A*, 2015, **3**, 1569–1579.

35 W. X. Zhang, Z. Q. Shan, K. L. Zhu, S. Z. Liu, X. Y. Liu and J. H. Tian, *Electrochim. Acta*, 2015, **153**, 385–392.

36 Y. Hong, Z. L. Tang and Z. T. Zhang, *Electrochim. Acta*, 2015, **176**, 369–377.

37 Y. Hong, Z. L. Tang, S. T. Wang, W. Quan and Z. T. Zhang, *J. Mater. Chem. A*, 2015, **3**, 10267–10274.

38 J. N. Zhu, W. C. Li, F. Cheng and A. H. Lu, *J. Mater. Chem. A*, 2015, **3**, 13920–13925.

39 H. Guo, C. Y. Wu, L. H. Liao, J. Xie, S. C. Zhang, P. Y. Zhu, G. S. Cao and X. B. Zhao, *Inorg. Chem.*, 2015, **54**, 667−674.

40 Q. B. Xia, T. Liu, J. J. Xu, X. Y. Cheng, W. Lu and X. D. Wu, *J. Mater. Chem. A*, 2015, **3**, 6301–6305.

41 J. G. Zheng, C. C. Qin, T. F. Wu, S. F. Xie, L. Ni, M. Y. Peng, Y. F. Tang and Y. F. Chen, *J. Mater. Chem. A*, 2015, **3**, 15299–15306.

42 J. G. Zheng, L. Ni, Y. W. Lu, C. C. Qin, P. X. Liu, T. F. Wu, Y. F. Tang and Y. F. Chen, *J. Power Sources*, 2015, **28**2, 444–451.

43 S. F. Yang, P. Y. Zavalij and M. S. Whittingham, *Electrochem. Commun.*, 2001, **3**, 505–508.

44 M. K. Devaraju and I. Honma, *Adv. Energy Mater.*, 2012, **2**, 284–297.

45 D. Choi, D. H. Wang, I. T. Bae, J. Xiao, Z. M. Nie, W. Wang, V. V. Viswanathan, Y. J. Lee, J. G. Zhang, G. L. Graff, Z. G. Yang and J. Liu, *Nano Lett.*, 2010, **10**, 2799–2805.

46 G. Y. Chen, A. K. Shukla, X. Y. Song and T. J. Richardson, *J. Mater. Chem.*, 2011, **21**, 10126–10133.

47 Y. S. Yu, C. Kim, D. A. Shapiro, M. Farmand, D. N. Qian, T. Tyliszczak, A. L. David Kilcoyne, R. Celestre, S. Marchesini, J. Joseph, P. Denes, T. Warwick, F. C. Strobridge, C. P. Grey, H. Padmore, Y. S. Meng, R. Kostecki and J. Cabana, *Nano Lett.*, 2015, **15**, 4282–4288.

48 S. S. Jan, S. Nurgul, X. Q. Shi, H. Xia and H. Pang, *Electrochim. Acta*, 2014, **149**, 86–93.

49 X. Tang, S. S. Jan, Y. Y. Qian, H. Xia, J. F. Ni, S. V. Savilov and S. M. Aldoshin, *Sci. Rep.*, 2015, **5**, 11958.

50 J. P. Schmidt, T. Chrobak, M. Ender, J. Illig, D. Klotz and E. Ivers Tiffée, *J. Power Sources*, 2011, **196**, 5342−5348.

51 J. Illig, M. Ender, T. Chrobak, J. P. Schmidt, D. Klotz and E. Ivers Tiffée, *J. Electrochem. Soc.*, 2012, **159**, A952−A960.

52 J. Illig, J. P. Schmidt, M. Weiss, A. Weber and E. Ivers Tiffée, *J. Power Sources*, 2013, **239**, 670–679.

53 K. S. Lee, K. J. Lee, Y. S. Kang, T. J. Shin, Y. E. Sung and D. Ahn, *Nanoscale*, 2015, **7**, 13860–13867.

54 H. J. Zhu, W. Zhai, M. Yang, X. M. Liu, Y. C. Chen, H. Yang and X. D. Shen, *RSC Adv.*, 2014, **4**, 25625–25632.

# Table of Contents entry

Nano-LiMnPO$_4$/C exhibits superior rate capability and long cycling stability sustaining a stable cycling of 500 cycles at 10 C.